www.ietdl.org

Published in IET Power Electronics
Received on 1st August 2013
Accepted on 7th March 2014
doi: 10.1049/iet-pel.2014.0014

ISSN 1755-4535

Comprehensive physically based modelling and simulation of power diodes with parameter extraction using MATLAB

Ahmed Shaker[1], *Mohamed Abouelatta*[2], *Gihan Taha Sayah*[3], *Abdelhalim Zekry*[2]

[1]*Department of Engineering Physics and Mathematics, Faculty of Engineering, Ain Shams University, Cairo, Egypt*
[2]*Department of Communications and Electronics, Faculty of Engineering, Ain Shams University, Cairo, Egypt*
[3]*Department of Electronic Engineering, Nuclear Materials Authority, Cairo, Egypt*
E-mail: gtsayah@hotmail.com

Abstract: In this study, we present an improved comprehensive model of power diodes. This model is based on the numerical solution of the ambipolar diffusion equation (ADE) by a modified finite difference method using MATLAB. The ADE is solved for all levels of injection instead of high-level injection only as usually done. Local physical effects such as conductivity modulation, emitter recombination, carrier–carrier scattering and lifetime control are taken into consideration. Temperature and self-heating effects are also included in the model. The proposed model has been validated against Silvaco mixed-mode simulations showing very good agreement with much less simulation times for our model. To be self contained, we also present a model parameter extraction methodology for power diodes given their experimental transient waveforms.

1 Introduction

For solving power electronic circuits one needs powerful and efficient circuit models of the power devices. These models must describe the terminal performance accurately under all practical operating conditions with the lowest computational loads on computing platforms. In addition their model parameters must be easily extracted from the measured characteristics of the device. Moreover they can be easily integrated into one of the existing software packages for solving power electronic circuits. For model generality and accuracy, the physically based models are the most appropriate. However, they may be complicated and have heavy computational loads. The use of the device simulator as Silvaco imparts the highest computational load, but gives the highest accuracy. So the circuit device modelling engineer efforts are continuously directed to find out device circuit models with reduced complexity and acceptable accuracy while preserving the generality.

The main difficulty in designing a physically based model for power diodes is in the distributed nature of the charge transport in the semiconductor which could be described using the ambipolar diffusion equation (ADE). The ADE could be solved using Laplace transforms [1], internal approximation [2], Fourier series [3, 4], finite element [5] or finite difference methods (FDMs). In our work, we will be concerned with the FDM-based modelling.

The FDM has been adopted a lot for solving the ADE. This method was first developed for a power diode model by Berz *et al.* [6]. In the FDM-based models, local effects such as conductivity modulation, carrier–carrier scattering, Auger recombination and the emitter recombination effects could be included [7, 8]. A model implemented in PSpice was proposed by Buiatti *et al.* [9], with much smaller computation times simulations than Silvaco [10] ones. The overall work of this model could be found in [11, 12]. However, all these models do not include temperature or self-heating effects. In addition, none of these FDM-based models provide a parameter extraction sequence.

Our approach in this paper is to extend the work of the FDM-based model to obtain an unconditionally stable solution that does not, to a high extent, depend on choosing the discretised mesh in space or the time step used in simulations. This approach was firstly presented in [13], but using limited effects. The model presented here solves the ADE under all injection levels by using a variable lifetime scheme. The model includes the important local physical effects like conductivity modulation, carrier–carrier scattering and the emitter recombination. In addition, the model includes the effect of localised lifetime that has been widely applied to optimise the switching characteristics of devices [14]. The temperature and self-heating effects are also included.

The model is implemented to obtain an accurate representation of the plasma movement in the reverse-recovery process and other physical effects. Describing the internal physical effects accurately facilitates the extraction of the design parameters especially when we do not use any unphysical fitting parameters. The novelty of the extraction procedure presented here is that we extract the physical parameters without incorporation of circuit parameters.

The general-purpose mathematical and numerical programming software MATLAB [15] is suitable for

optimisation of parameters extraction sequences of the device under investigation. Therefore we chose MATLAB as an implementation tool for this model. There exists a MATLAB connection to Powersim [16] which is a software package used in solving the power electronics circuits and so our MATLAB model can be integrated in such a package. In another paper [17], we presented the implementation in PSpice as RC network with some dependent sources.

The paper is organised as follows. In Section 2, the basics of the model are summarised and the model equations reviewed. In Section 3, the proposed FDM scheme is discussed. In Section 4, comparisons between simulations and Silvaco TCAD results are presented. Finally, a parameter extraction procedure is offered and two case studies are presented to extract the design parameters using measurements data.

2 Model description

2.1 Main assumptions

The power diode considered here is composed of three regions: the cathode, the anode and the base regions. The cathode is a highly n-doped region (N^+), the base region is a lightly n-doped region (N^-) and the anode is a highly p-doped region (P^+). The base region width is W_B and its concentration is N_D with a high-level lifetime τ_{hl} and a low-level lifetime τ_{ll}. The lifetime at the base may be variable as the case of localised lifetime control. The charge storage region (CSR) contains the excess carriers during the on-state where there are no depletion layers. During turn-off, the depletion layers spread out from the ends of the base region [18] as shown in Fig. 1. The figure also shows the variation of τ_{hl} for a non-homogeneous lifetime scheme (for homogeneous lifetime: $\tau_1 = \tau_2 = \tau_{hl}$).

2.2 Basic equations

In the quasi-neutral base region, one can assume

$$n(x) = p(x) + N_D \tag{1}$$

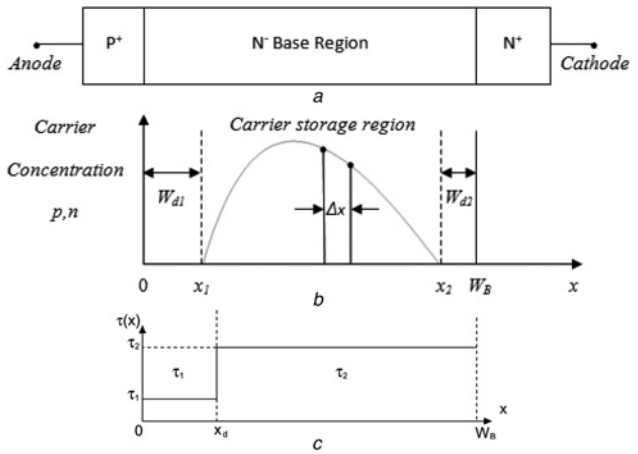

Fig. 1 *Main assumptions*

a Basic power diode structure
b Carrier concentration in the base width during a turn-off process, showing the depletion widths W_{d1} and W_{d2}
c Variation of τ_{hl} for a non-homogeneous lifetime scheme

where $n(x)$ and $p(x)$ are the concentrations of electrons and holes, respectively. The ADE for all levels of injection can be approximated as follows [19]

$$\frac{\partial p}{\partial t} = -\frac{p - p_o}{\tau_{SRH}} + D_a \frac{\partial^2 p}{\partial x^2} \tag{2}$$

where p_o is the equilibrium hole concentration and D_a is the ambipolar diffusion constant

$$D_a = D_n \frac{p + n}{bn + p} \tag{3}$$

The mobility ratio $b = \mu_n/\mu_p = D_n/D_p$, where μ_n and μ_p are the electron and hole mobilities and D_n and D_p are the electron and hole diffusion constants, respectively. In (2), we neglect Auger recombination as long as the current density does not exceed 100 A/cm^2 [20]. On the basis of the Shockley–Read–Hall model, the lifetime τ_{SRH} can be written as [19, 21]

$$\tau_{SRH} \simeq \frac{(n - N_D)\tau_{hl} + N_D \tau_{ll}}{(n)} \tag{4}$$

The boundary conditions for (2) at $x = x_1$ and $x = x_2$ (where $x_1 = W_{d1}$ and $x_2 = W_B - W_{d2}$ are the left and right borders of the region flooded with excess carriers) are [19]

$$\frac{\partial p}{\partial x}(x = x_1) = -\frac{I_D}{qAD_p}\frac{n}{p + n} + \frac{I_n(x = x_1)}{qAbD_p}\frac{p + bn}{p + n} \tag{5a}$$

$$\frac{\partial p}{\partial x}(x = x_2) = \frac{I_D}{qAbD_p}\frac{p}{p + n} - \frac{I_p(x = x_2)}{qAbD_p}\frac{p + bn}{p + n} \tag{5b}$$

In (5), I_D is the total diode current, I_n is the electron current, $I_p$is the hole current, A is the device area and q is the electronic charge. The corresponding electron and hole currents could be approximated as follows [18]

$$I_n(x = x_1) = qAh_n p^2_{(x=x_1)} - qAN_D \frac{\partial x_1}{\partial t} \tag{6a}$$

$$I_p(x = x_2) = qAh_n p^2_{(x=x_2)} - qAN_D \frac{\partial x_2}{\partial t} \tag{6b}$$

The first term in (6) corresponds to the end region recombination where h_n and h_p are the recombination parameters; the second one is the displacement current.

To calculate the total voltage drop, we divide it into several terms. In the absence of punch-through, the depletion layer voltage is the sum of the following equations [11, 12]

$$V_{d1} = \frac{q}{2\varepsilon}\left(N_D + \frac{|I_{p1}|}{qA\upsilon_{sat}}\right) \times W_{d1}^2 \tag{7a}$$

$$V_{d2} = \frac{q}{2\varepsilon}\left(N_D + \frac{|I_{p2}|}{qA\upsilon_{sat}}\right) \times W_{d2}^2 \tag{7b}$$

where V_{d1} and V_{d2} are the voltages across the depletion layers W_{d1} and W_{d2}, respectively. I_{p1} and I_{p2} are the hole currents at the respective boundaries x_1 and x_2. The space-charge includes the ionised impurities N_D and the density of free carriers injected in the depleted regions assuming a

saturated drift velocity condition (where v_{sat} is the hole high field saturation velocity).

The junction voltages are given by Igic *et al.* [22]

$$V_{j1} = V_T \ln\left(\frac{p_{x1}}{n_i} + \frac{n_i}{N_D}\right) \tag{8a}$$

$$V_{j2} = V_T \ln\left(\frac{p_{x2} + N_D}{n_i}\right) \tag{8b}$$

The voltage drop across the lightly doped drift region can be calculated following the approach in [11] as follows

$$V_B = \frac{I_D}{qA} \sum_{i=1}^{N} \frac{\Delta x}{p_i(\mu_n + \mu_p) + \mu_n N_D} \tag{9}$$

where N is the number of discretised elements and Δx is the width between two elements (as shown in Fig. 1). Mobility degradation effect, because of electron–hole scattering could be added by assuming that [11]

$$\mu_n + \mu_p = \frac{n_o \mu_o}{n + n_o} \tag{10}$$

where μ_o and n_o are suitable constants.

Finally, the total diode voltage can be calculated by summing the relevant voltages

$$V_{AK} = V_{j1} + V_{j2} + V_B - V_{d1} - V_{d2} \tag{11}$$

3 FDM scheme

There are a lot of FDM schemes in the literature [6–12]. We here consider the forward time central space scheme, where the time derivative operator is discretised by forward Euler method and the space derivative by central Euler method. The regular implementation of this method has a drawback in its conditional stability [23]. To assure the stability of our implemented method, we use a variable time step of the simulation.

Considering the grid of the solution, there are two methods: the fixed and movable grid. For the fixed grid, the diode base region is discretised into fixed number of points. The fixed grid as in [6–8] has the advantage of simple calculations for carrier concentration, but the drawback comes from the calculation of the depletion regions because it assumes that the ADE solution ends at two fixed points. Therefore the solution may choose points that do not represent accurately the depletion region widths because of the limited number of fixed points.

The movable grid as in [11] has the advantage of accurately tracing the depletion region width. Unfortunately, the solution of the carrier concentration could be less accurate. The regular solution of the movable grid is based on computing the carrier concentration in a time step over the CSR using the previous time step which, actually, may be calculated at different space points. We found that this leads to accumulative errors which cannot be ignored and usually result in bad extraction of design parameters.

In our model, we use a movable grid method and modify the way to calculate the carrier concentration. When calculating the carrier concentration at a time step, we obtain the solution of the previous time step at the same space points of this current time step (by interpolation) as schematically depicted in Fig. 2.

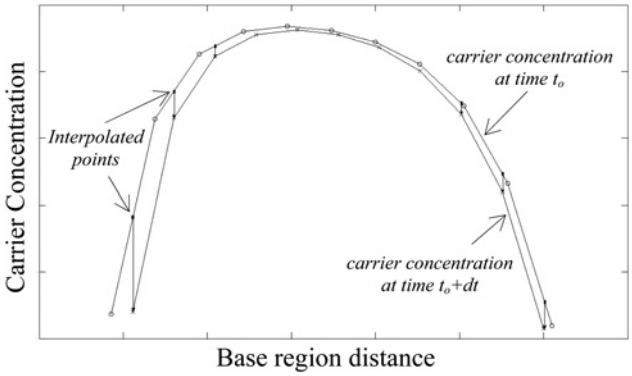

Fig. 2 *Calculation of carrier concentration based on finding interpolated points of previous time step to obtain current time step solution*

The calculation of the depletion regions are specified following [6]. We found from extensive simulations, using Silvaco, that the depletion region which enhances the electric field actually lies between the P^+ N^- interface and the point at which $n = p$ at the left and right boundaries given by Berz *et al.* [6]

$$n(x_1,\ t) = K|J| \tag{12a}$$

$$n(x_2,\ t) = (K/b)|J| \tag{12b}$$

where

$$K \simeq \frac{(1.04 \times 10^{20})}{N_D^{1/2}} \tag{12c}$$

4 Model validation

A one-dimensional p^+–n^-–n^+ diode structure similar to [24] is used to validate our model. The doping profile is characterised by a base region doping of $N_D = 6.4 \times 10^{13}\ cm^{-3}$, a diode thickness of 130 μm and identical Gaussian profiles of the P^+- and N^+-regions (with $N_{Peak} = 2 \times 10^{17}\ cm^{-3}$ and junction depth = 5 μm), the corresponding base region width W_B is 120 μm. The area A is taken to be 1 cm^2, $\tau_{hl} = 13$ μs and $\tau_{ll} = 3$ μs.

To study the reverse-recovery behaviour, we use a circuit which is an idealised model of the boost converter topology, widely used in the literature [25]. The boost converter is shown in Fig. 3*a*. If the boost converter works in the continuous current mode, the inductance L can be approximated with a constant current source I_F and the output capacitor behaves as a voltage source V_{rev} [25, 26]. In addition, the switch is idealised and the turn-off is

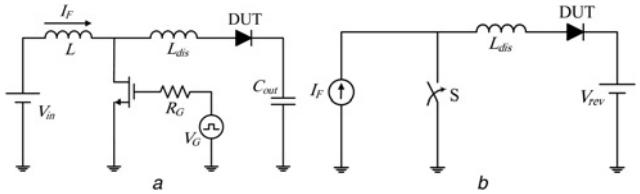

Fig. 3 *Test circuit used in the reverse-recovery simulations*

a Boost converter
b Corresponding idealised circuit

doi: 10.1049/iet-pel.2014.0014

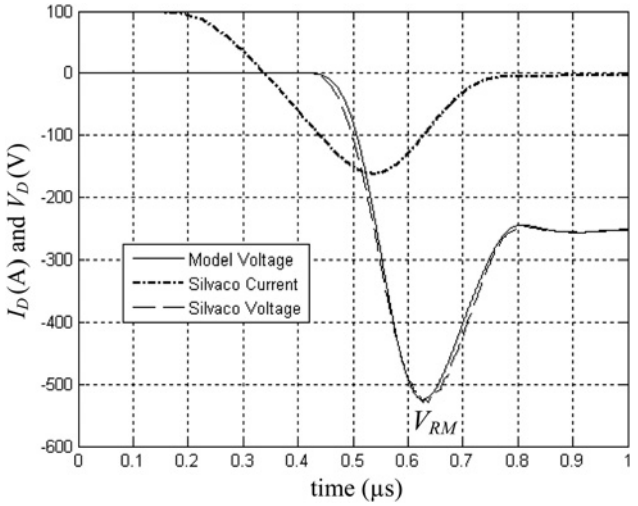

Fig. 4 *Current (using Silvaco) and voltage (using Silvaco and MATLAB) waveforms*

because of the presence of a distributed inductor L_{dis} which simulates parasitics as shown in Fig. 3*b*. Taking $L_{dis} = 0.25$ μH, Silvaco mixed-mode simulation is run and we obtain the transient current and voltage waveforms seen in Fig. 4.

To confirm that the design parameters match well for our model, we need to separate the circuit performance from the device performance. Therefore we use the current waveform as an input to the model implemented in MATLAB. Actually, this is a novel method to predict the design parameters without including the circuit complexity. Applying the current waveform and using the same design parameters as used in Silvaco simulations, we fit the voltage waveform as seen in Fig. 4 by adjusting the *h*-parameters. Values of $h_n = 34 \times 10^{-14}$ cm^4/s and $h_p = 48 \times 10^{-14}$ cm^4/s are adjusted for best fit.

To examine that our model is capable of tracing the internal physical quantities, we compare our results for the plasma formation with that obtained from Silvaco simulations. Fig. 5*a* shows the variation of the left depletion width W_{d1} and right depletion width W_{d2} with transient time. In addition, the complete hole distributions at certain times are shown in Fig. 5*b* for certain selected times. Considering Fig. 5*a*, the maximum relative error of W_{d1} is 6% and that of W_{d2} is 8%. In addition, considering Fig. 5*b*, the maximum relative error of the carrier concentration is 16%. We see that very good agreement is obtained either for terminal characteristics or internal physical behaviours.

Next, we study the effect of varying L_{dis} and maintaining all other parameters fixed. The selected value is 0.35 μH. The result of the voltage waveform is shown in Fig. 6*a* proving that our model parameters are insensitive to circuit variations. The influence of the forward current I_F is also studied. We take $I_F = 50$ A at a value of $L_{dis} = 0.25$ μH. The voltage waveform obtained by our model which is shown in Fig. 6*b* was fitted to that of Silvaco using different but close values of *h*-parameters, namely $h_n = 30 \times 10^{-14}$ cm^4/s and $h_p = 55 \times 10^{-14}$ cm^4/s. Actually, we find that the model is very sensitive to *h*-parameters variations. In addition, we show how the variable lifetime model used is more accurate over the constant lifetime model mainly for low-level injection.

The variation of *h*-parameters according to I_F was not addressed before in all power diode models to our knowledge. We see that changing I_F results in changing

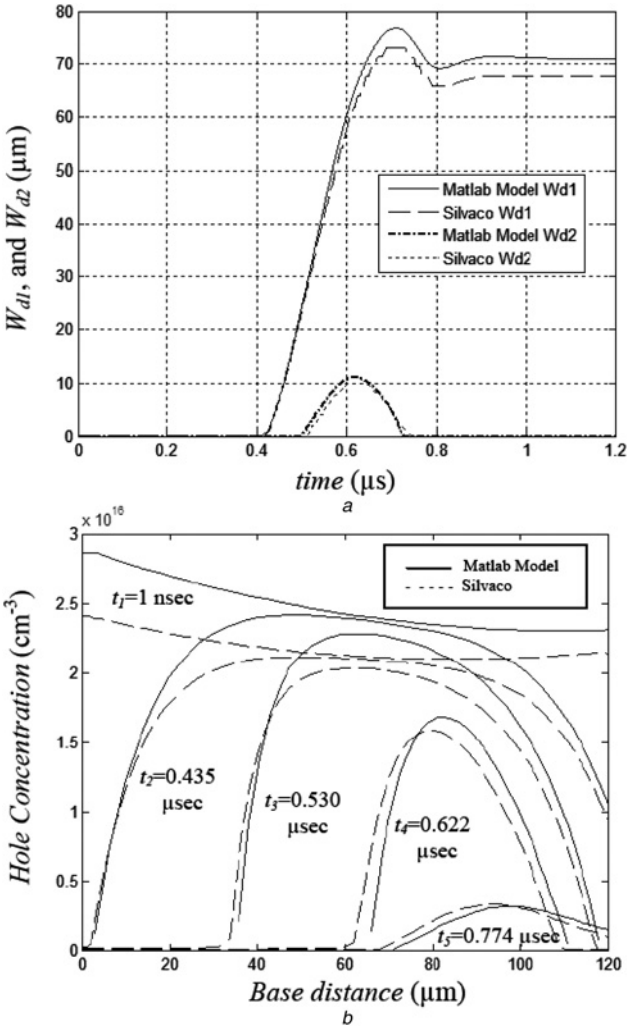

Fig. 5 *Model physical validation*

a Depletion widths W_{d1} and W_{d2}
b Hole concentration inside base region

h-parameters. This could be interpreted from the following equation [by approximating (7)]

$$h_p \simeq I_n(x = x_1)/qAp^2_{(x=x_1)} \tag{13a}$$

$$h_n \simeq I_p(x = x_2)/qAp^2_{(x=x_2)} \tag{13b}$$

Increasing the forward current I_F results in increasing the hole concentration at x_1 and x_2. In addition, the recombination currents (I_n at x_1 and I_p at x_2) will increase. Therefore (13) could not tell whether the *h*-parameters will increase or decrease. In our model, we found that as I_F increases h_n slightly increases while h_p decreases.

To study this trend, we found the corresponding recombination currents and hole concentrations using Silvaco and calculated the *h*-parameters using (13). Table 1 demonstrates the results. Comparing our model values with that obtained by Silvaco, we can see a good agreement for the phenomenon. Actually, the variation in h_n is very small compared with h_p variation. An experimental verification of these conclusions is found in [27].

Next, the effect of the doping of the emitters is considered to demonstrate the effect on the *h*-parameters. A doping of 2×10^{19} cm^{-3} was assumed for both sides. Changing the forward current I_F from 100 to 200 A, we fit the voltage

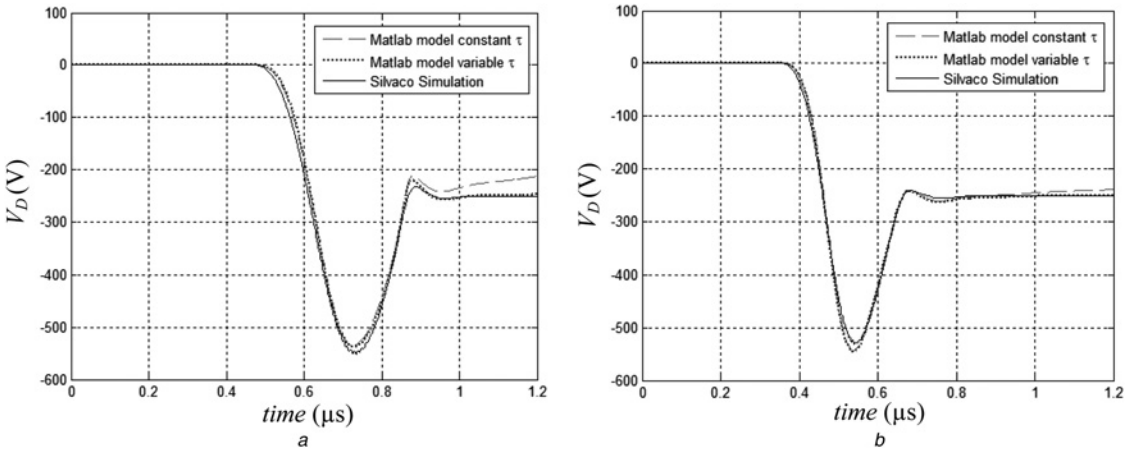

Fig. 6 *Voltage waveforms (using Silvaco and MATLAB)*
a $L_{dis} = 0.35$ μH
b $I_F = 50$ A

waveform by choosing $h_n = 2.75 \times 10^{-14}$ cm^4/s and $h_p = 2.85 \times 10^{-14}$ cm^4/s. The results are shown in Fig. 7. The variation of *h*-parameters with respect to the forward current was not notable because of the sharp variation of the doping at the emitter sides.

Finally, the effect of the temperature on the device performance is studied. A summary of the temperature dependence of model parameters is given in Table 2 [4]. Fig. 8*a* shows the voltage waveforms of both Silvaco and model results. The conditions simulated used are the same as the previous case: $I_F = 100$ A, $L_{dis} = 0.25$ μH and emitter doping of 2×10^{19} cm^{-3}. The temperature is kept at 450 K for this simulation. Additionally, Fig. 8*b* shows the DC characteristics of the device simulated at constant junction temperature of 300 K (isothermal) and including the self-heating effects (non-isothermal). The DC characteristic

Table 1 Variations of *h*-parameters because of variation of I_F

	Silvaco		MATLAB model	
I_F, A	50	100	50	100
h_p, cm^4/s	53.3×10^{-14}	51.1×10^{-14}	55×10^{-14}	48×10^{-14}
h_n, cm^4/s	29.2×10^{-14}	29.5×10^{-14}	30×10^{-14}	34×10^{-14}

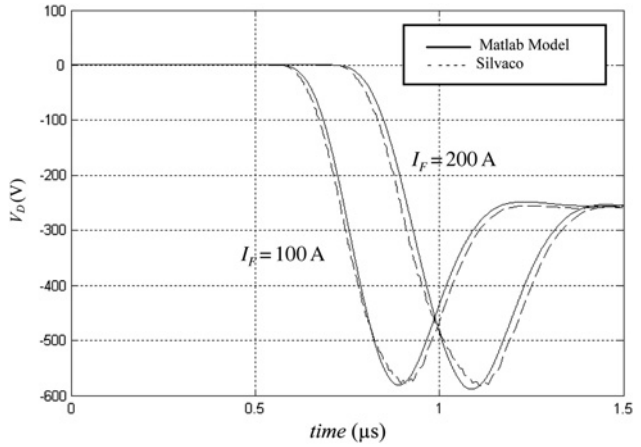

Fig. 7 *Voltage waveforms for $I_F = 100$ A and $I_F = 200$ A at $L_{dis} = 0.25$ μH and emitter doping of 2×10^{19} cm^{-3}*

Table 2 Temperature dependence of model parameters

Parameters	Temperature dependence equations
carrier lifetime	$\tau_{hl} = \tau_{hl300}\left(\frac{T}{300}\right)^{1.5}$
electron mobility	$\mu_n = 1350\left(\frac{300}{T}\right)^{2.5}$
hole mobility	$\mu_p = 495\left(\frac{300}{T}\right)^{2.2}$
intrinsic concentration	$n_i = 3.88 \times 10^{16}(T)^{1.5} / \exp\left(\frac{7000}{T}\right)$
recombination *h*-parameters	$h_{n,p} = h_{n,p300}\left(\frac{300}{T}\right)^{2.5}$

including self-heating effects is reported for an external thermal resistance of average value of 5 K/cm^{2}W. The proposed model simulations are in very good agreement with Silvaco.

Next, we compare the terminal characteristics of a turn-off example using our device parameters with the simulation results of Silvaco and another FDM-based model (by Buiatti *et al.* [11]). First, Fig. 9*a* shows the MATLAB model waveforms compared with Silvaco. As shown the results are in good agreement noting that the device parameters of both simulations are the same. Second, the terminal characteristics of Buiatti model using the device parameters without any fitting shows low accuracy as can be depicted from Fig. 9*b*. We try to fit the current and voltage waveform. Unfortunately, the physical parameters were changed substantially to match the waveforms.

The instantaneous power dissipation for all cases is shown in Fig. 9*c*. Considering Silvaco, the maximum power dissipation P_{max} is 64.94 kW at 0.5878 μs, whereas it is 66.08 kW at 0.5868 μs for our model. Considering Buiatti model, P_{max} is only 47.6 kW at 0.408 μs without fitting, whereas it is 74.35 kW at 0.5519 μs with fitting.

5 Parameter extraction procedure

The proposed model has been applied to extract the design parameters of a fast-recovery power diode RUR8100 (rated

doi: 10.1049/iet-pel.2014.0014

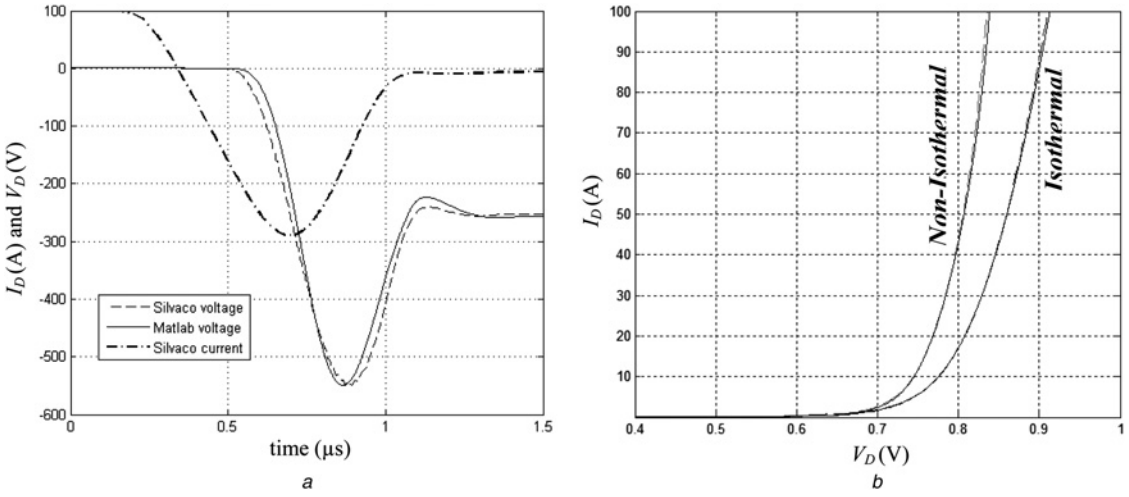

Fig. 8 *Temperature and self-heating effects*

a Current and voltage waveforms at $T = 450$ K
b DC characteristics: isothermal (at $T = 300$ K) and non-isothermal using Silvaco (dash lines) and MATLAB model (solid lines)

at 1 kV and 8 A). We use the experimental reverse-recovery waveforms from Strollo and Napoli [28]. An initial guess of parameters is done following [4, 29]. First, the current waveform is filtered and interpolated. Then, it is used as an input to the MATLAB model. An optimisation using MATLAB is applied to match the experimental voltage waveform with that of the model by varying the device parameters and obtaining the best fit.

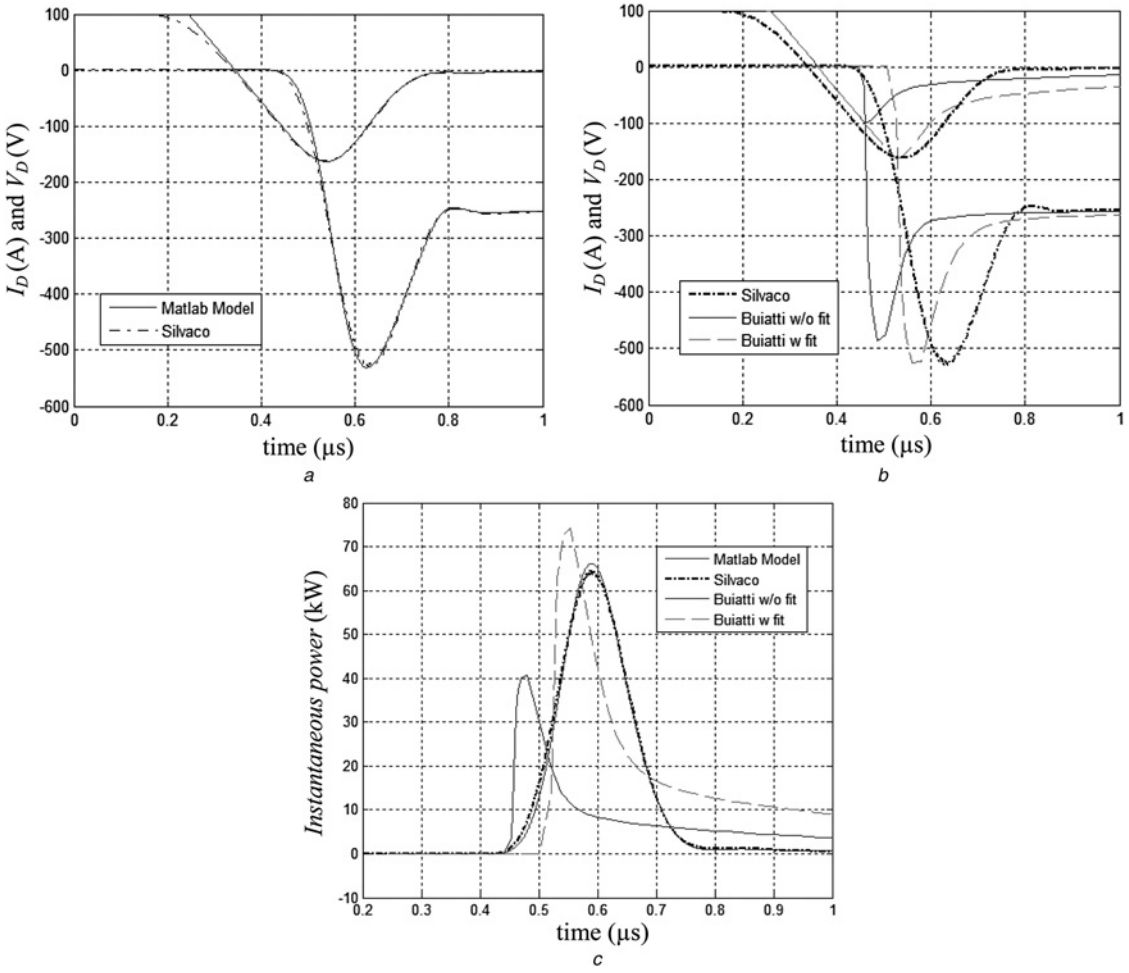

Fig. 9 *Transient waveforms comparison*

a Terminal characteristics using Silvaco and MATLAB
b Terminal characteristics using Silvaco and Buiatti model
c Instantaneous power

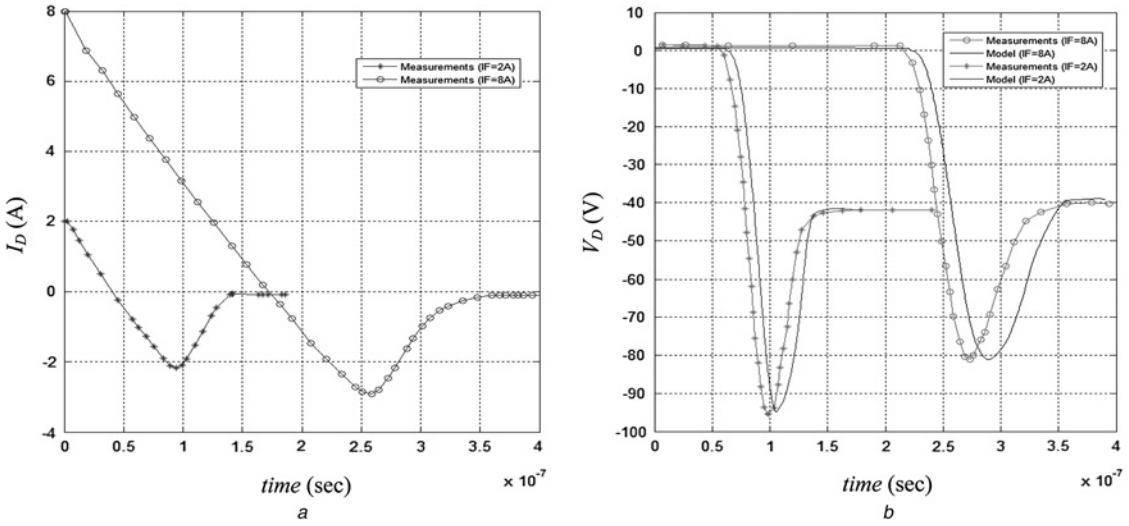

Fig. 10 *Experimental current waveforms and voltage waveforms both experiment and using MATLAB model*

a Current
b Voltage

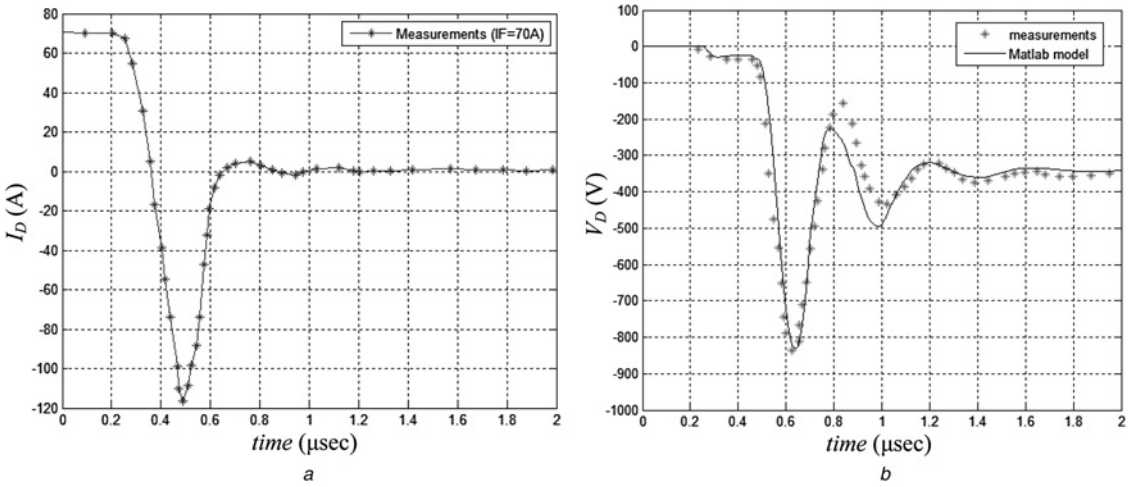

Fig. 11 *Experimental current and voltage waveforms both experiment and using MATLAB model*

a Current
b Voltage

Fig. 10*a* shows the experimental current waveforms for $I_F = 8$ A and 2 A with $di/dt \simeq 46$ A/μs. The corresponding voltage waveforms by means of MATLAB and experimental results are shown in Fig. 10*b*. For the case of $I_F = 2$ A, we obtain the best fit for voltage waveform by adjusting $W_B = 110$ μm, $N_D = 1.24 \times 10^{14}$ cm^{-3}, $\tau_{hl} = 155$ ns, $\tau_{ll} = 90$ ns, $A = 0.08$ cm^2 and $h_p = h_n = 1 \times 10^{-14}$ cm^4/s. To validate these values, we apply another reverse-recovery process with different circuit conditions at $I_F = 8$ A. The results indicate that there is a very good match between simulation and experiment. The delay in the voltage waveform is because of the assumption of constant width as the emitters are assumed boxed type which is not the actual case.

Another case study for a Powerex device (CS240610) rated at 600 V/100 A. This power diode is proved to have a local lifetime control [30]. The base width (W_B), lifetime profile ($\tau_{hl(low)}$, x_d and $\tau_{hl(high)}$) and area (A) were fixed at the values given in [30]. The other parameters (N_D, h_p and h_n) are varied to achieve the best fit of the experimental voltage waveform. Fig. 11*a* shows the experimental current waveform and Fig. 11*b* shows the corresponding voltage waveform by means of MATLAB and experimental results. We obtain the best fit by adjusting $N_D = 1 \times 10^{14}$ cm^{-3}, $h_p = 3.5 \times 10^{-14}$ cm^4/s and $h_n = 3 \times 10^{-14}$ cm^4/s. The voltage oscillations are not properly fitted because of the lack of accuracy in extracting the measured current for small values of the current.

6 Conclusions

In this paper, a physically based model of the power diode using MATLAB has been presented. The model solves the ADE numerically using a modified FDM. The model takes the basic local physical effects into consideration and provides a comprehensive physical and circuit insight about the operation of the power diode. The presented model allows many operating conditions to be studied rapidly, to certify reliable operation. Some case studies to validate the model accuracy were performed and the results were

doi: 10.1049/iet-pel.2014.0014

compared with Silvaco mixed-mode simulations showing very good agreement with much less simulation times for our model.

We also introduced a new parameter extraction procedure by using the model as a tool in refining the design parameters of the power diode. This could be done by input the measured current waveform of a reverse-recovery process to the model and optimising the design parameters to obtain the best fit of the voltage waveform compared with experiment. Two case studies were presented and good agreement between simulations and measurements were obtained.

7 References

1 Strollo, A.G.M.: 'SPICE modeling of power PiN diode using asymptotic waveform evaluation'. PESC Conf. Record, Baveno, 1996, pp. 44–49
2 Allard, B., Morel, H., Chante, J.-P.: 'Reusing basic semiconductor region models in power device bond graph definition'. EPE Conf. Record, Brighton, 1993, pp. 34–39
3 Leturcq, Ph., Berraies, M.O., Debrie, J-L, Gillet, P., Kallala, M.A., Massol, J-L: 'Bipolar semiconductor device models for computer-aided design in power electronics'. EPE Conf. Record, Seville, 1995, pp. 222–227
4 Palmer, P.R., Santi, E., Hudgins, J.L., Kang, X., Joyce, J.C., Eng, P.Y.: 'Circuit simulator models for the diode and IGBT with full temperature dependent features', *IEEE Trans. Power Electron.*, 2003, **18**, (5), pp. 1220–1229
5 Chibante, R., Araujo, A., Carvalho, A.: 'A new approach for physical-based modelling of bipolar power semiconductor devices', *Solid-State Electron.*, 2008, **52**, pp. 1766–1772
6 Berz, F., Pritchard, J., Crowley, A.B.: 'Modeling PIN diode switch-off with the enthalpy method', *Solid-State Electron.*, 1984, **27**, (8/9), pp. 769–774
7 Goebel, H.: 'A unified method for modeling power semiconductor devices', *IEEE Trans. Power Electron.*, 1994, **9**, (5), pp. 497–505
8 Metzner, D., Vogler, T., Schroeder, D.: 'A modular concept for the circuit simulation of bipolar power semiconductors', *IEEE Trans. Power Electron.*, 1994, **9**, (5), pp. 506–513
9 Buiatti, G.M., Cappelluti, F., Ghione, G.: 'Finite difference based power diodes simulation within SPICE: modeling approach and validation'. IEEE PESC'05, 2005, pp. 999–1003
10 www.silvaco.com
11 Buiatti, G.M., Cappelluti, F., Ghione, G.: 'Physics-based PiN diode SPICE model for power-circuit simulation', *IEEE Ind. Appl. Trans.*, 2007, **43**, (4), pp. 911–919
12 Buiatti, G.M.: 'Modeling and simulation of power PiN diodes within SPICE'. PhD thesis, Politecnico di Torino, 2006
13 Shaker, A., Zekry, A., Omar, O.A., Gamal, S.: 'An improved power diode model based on finite difference method'. Proc. Second Int. Conf. on Advanced Computer Theory and Engineering (ICACTE'09), Cairo, Egypt, 2009, pp. 659–670
14 Temple, V.A.K., Holroyd, F.W.: 'Optimizing carrier lifetime profile for improved trade-off between turn-off time and forward drop', *IEEE Trans. Electron Devices*, 1983, **ED-30**, pp. 782–790
15 www.mathworks.com
16 http://www.powersimtech.com/products/psim/
17 Shaker, A., Zekry, A.: 'A modified PSPICE model for the power PIN diode'. IEEE 22nd Int. Conf. Microelectronics, Cairo, Egypt, 2010
18 Bryant, A.T.: 'Simulation and optimization of diode and IGBT interaction in a chopper cell'. PhD thesis, Queens' College, University of Cambridge, 2005
19 Di Zitti, E., Bisio, G.M.: 'Determination of silicon power diode recombination parameters by combining open circuit voltage decay and storage time reverse recovery data', *Solid-State Electron.*, 1991, **37**, (7), pp. 771–780
20 Ghandhi, S.K.: 'Power semiconductor devices' (Wiley, New York, 1977)
21 Moll, J.L.: 'Physics of semiconductors' (McGraw-Hill, New York, 1964)
22 Igic, P.M., Mawby, P.A., Towers, M.S., Batcup, S.: 'New physically-based PiN diode compact model for circuit modeling applications', *IEE Proc. Circuits Devices Syst.*, 2002, **149**, (4), pp. 257–263
23 Riley, K., Hobson, M., Bence, S.J.: 'Mathematical methods in engineering and physics', (Cambridge University Press, Cambridge, United Kingdom, 2002)
24 Baburske, R., Heinze, B., Lutz, J., Niedernostheide, F.: 'Charge-carrier plasma dynamics during the reverse-recovery period in p^+–n^-–n^+ diodes', *IEEE Trans. Electron Devices*, 2008, **55**, (8), pp. 2164–2172
25 Napoli, E., Strollo, A.G.M., Spirito, P.: 'Numerical analysis of local lifetime control for high-speed low-loss P–i–N diode design', *IEEE Trans. Power Electron.*, 1999, **14**, (4), pp. 615–621
26 Schlangenotto, H., Fullmann, M.: 'A hybrid fast power diode with strongly improved reverse recovery'. Proc. EPE Conf., 1993, pp. 185–190
27 Berz, F., Cooper, W., Fagg, S.: 'Recombination in the end regions of pin diodes', *Solid-State Electron.*, 1979, **22**, pp. 293–301
28 Strollo, A.G.M., Napoli, E.: 'Improved PIN diode circuit model with automatic parameter extraction technique', *IEE Proc., Circuits Devices Syst.*, 1997, **144**, pp. 329–334
29 Cova, P., Delmonte, N., Bertoluzza, F.: 'A software tool for the design of high power PiN diodes based on the numerical study of the reverse characteristics', *Solid-State Electron.*, 2011, **63**, pp. 60–69
30 Lu, L., Bryant, A.T., Santi, E., Palmer, P.R., Hudgins, J.L.: 'Physical modeling of fast p–i–n diodes with carrier lifetime zoning, part II: parameter extraction', *IEEE Trans. Power Electron.*, 2008, **23**, (1), pp. 198–205